J Fluoresc (2013) 23:393–398
DOI 10.1007/s10895-013-1202-1

SHORT COMMUNICATION

Detection of Volume Changes in Calcein-Stained Cells Using Confocal Microscopy

Allyson Fry Davidson · Adam Z. Higgins

Received: 3 December 2012 / Accepted: 24 February 2013 / Published online: 7 March 2013

Abstract Calcein is an intracellular fluorescent probe that has been used as an indicator of cell volume in several previous studies. These studies have reported two different fluorescence responses depending on the optical setup used to collect the data: wide-field microscopy has resulted in a decrease in fluorescence upon cell shrinkage, whereas confocal microscopy has been shown to yield the opposite result. In this short communication, we have investigated the effect of optical setup on detection of cell volume changes in calcein-stained endothelial cells. A confocal microscope was used to collect the fluorescence data, and the pinhole diameter was varied in order to examine the effects of optical section thickness on fluorescence response. For large pinhole diameters – which correspond to relatively thick optical sections – fluorescence intensity decreased when cells were induced to shrink. In contrast, for small pinhole diameters the fluorescence intensity increased with cell shrinkage. The transition between these two types of fluorescence responses occurred when using a pinhole diameter of 285 μm, which corresponds with an optical section thickness slightly less than the height of the cells. Our results have implications for the design and interpretation of experiments involving the use of calcein as a cell volume indicator.

Keywords Cell membrane permeability · Fluorescence quenching · Optical section thickness · Calcein

A. F. Davidson · A. Z. Higgins (✉)
School of Chemical, Biological and Environmental Engineering,
Oregon State University, 102 Gleeson Hall,
Corvallis, OR 97331-2702, USA
e-mail: adam.higgins@oregonstate.edu

Introduction

Measurement of the dynamics of cell volume changes is important in several areas, including investigation of cell membrane permeability [1] and regulatory volume changes [2, 3]. Several methods have been developed to detect volume changes in adherent cells (reviewed in [2]). In particular, calcein has been used as a volume indicator in several previous studies [4–15]. To load calcein into cells, a nonfluorescent calcein derivative, calcein acetoxymethyl ester (calcein-AM) is typically used. Calcein-AM readily crosses the cell membrane, but once inside the cell, the acetoxymethyl functional group is hydrolyzed by intracellular esterases, leaving the fluorescent and membrane impermeable calcein molecule trapped inside the cell.

Two conflicting relationships between cell volume and calcein fluorescence have been reported in the literature. Studies using wide-field epifluorescence microscopy have reported a decrease in fluorescence when cells shrink after exposure to hypertonic solution [4–6, 9, 11–13, 16]. This decrease in fluorescence has been attributed to quenching of calcein fluorescence by endogenous molecules present in the cytoplasm [14]. However, when using confocal microscopy an increase in fluorescence is detected when cells shrink [7, 15, 17, 18]. The increase in fluorescence has been attributed to an increase in the intracellular concentration of calcein. These conflicting results raise questions on the validity and limitations of the two imaging methods, and we have not been able to locate direct comparisons of the two methods in the literature.

We have previously used calcein as a volume indicator in wide-field epifluorescence microscopy experiments to measure the permeability properties of cultured endothelial cells [19]. These experiments were undertaken with the goal of

developing new cryopreservation strategies for adherent cells and tissues. Mathematical models of cell membrane transport have previously been used to rationally design cryopreservation procedures [20–23]. However, it is particularly challenging to apply these rational design strategies to three-dimensional tissues because there are not convenient methods for measuring the permeability properties of cells within tissue. Consequently, one of our long-term goals is to adapt the calcein-based method that we used with adherent endothelial cells [19] for use with three-dimensional tissues. This will require an understanding of the differences between confocal and wide-field imaging when using calcein as a cell volume indicator.

The purpose of this study was to investigate the effect of optical setup on the response of calcein fluorescence during cell shrinkage. Cultured endothelial cells were exposed to hypertonic solution in a simple microfluidic chamber while simultaneously collecting fluorescence images with a confocal microscope. Images were acquired while varying the detector pinhole aperture such that images acquired with a minimum pinhole diameter were true confocal images, but images acquired with a maximum pinhole diameter approximated those collected with a wide-field epifluorescence microscope. Our results clarify the effects of confocal and wide-field imaging modalities on the fluorescence response of calcein-loaded cells, and provide information that will facilitate the adaptation of calcein-based methods for determination of membrane permeability in three-dimensional tissue.

Methods

Cell Culture

Cell culture supplies were purchased from Invitrogen (Carlsbad, CA) unless otherwise noted. Bovine pulmonary artery endothelial cells (Cambrex, San Diego, CA) were cultured on tissue culture treated plastic T25 flasks in a 5 % CO_2 environment at 37 °C. The culture medium was composed of Dulbecco's Modified Eagle Medium low glucose nutrient mixture supplemented with 5 % v/v fetal bovine serum, 100 U/ml penicillin, and 100 μg/mL streptomycin in cell culture grade UltraPure water (ThermoFisher, Waltham, MA). Medium was changed every 48 h. Flasks were subcultured when they reached approximately 80 % confluency and split at a ratio of 1:5 using 0.05 % trypsin-EDTA solution. To prepare samples for experiments, 25 mm diameter glass coverslips were placed into separate 30 mm petri dishes and sterilized with 70 % ethanol. Cells were seeded onto coverslips at a density of 1×10^5 cells per coverslip and cultured for 3 days before experimentation, at which point they had reached a confluency of 80 %.

Perfusion Chamber

To create the perfusion chamber, two pieces of acrylic, 2.25 mm and 9.25 mm in thickness, were first cut to be approximately 6 cm × 10 cm. An imaging window was created by drilling a 3/4 in. hole in the center of the thinner acrylic piece. Inlet and outlet ports were inserted into the thicker acrylic piece so that they were flush with the top surface of the acrylic. A gasket of 100 μm thick medical grade silicone (BioPlexus, Ventura, CA) with a 3 mm × 15 mm (width × length) cutout was adhered to the thicker acrylic piece, aligning the cutout with the fluidic ports. To assemble the chamber, a 25 mm coverslip with cultured cells was inverted onto the silicone gasket. The thinner acrylic piece with the imaging window and a matching 1/16 in. ethylene-vinyl acetate foam gasket was placed on top and the assembled perfusion chamber was held firmly together with foldover clips. Solutions were delivered to the chamber with dual computer-controlled NE-500 OEM syringe pumps (New Era Pump Systems, Farmingdale, NY). The inlet port was attached to a Y connector which enabled delivery of alternating isotonic and hypertonic test solutions using the dual syringe pumps.

Experimental Solutions

Isotonic (300 mOsm/kg) Dulbecco's phosphate buffered saline with calcium and magnesium (PBS) was made in-house. Hypertonic solution was prepared by adding sucrose (Mallinkrodt, Hazelwood, MO) to the isotonic PBS to create a solution osmolality of 1000 mOsm/kg. The actual osmolalities were confirmed to be within 1 % of the nominal values using a freezing point depression osmometer (Advanced Micro Osmometer Model 3300, Advanced Instruments, Norwood, MA).

Confocal Microscopy

To prepare endothelial cells for fluorescence imaging, coverslips were treated with a solution of 1.25 μg/mL calcein-AM (Sigma Aldrich, St. Louis, MO) in isotonic PBS for 15 min at 37 °C. Coverslips were assembled into the perfusion chamber which was then placed onto the Axiovert 200 motorized stage of a Zeiss LSM 510 Meta confocal microscope. An argon laser at 6.1 Amps and 1 % intensity was used as the excitation source. All imaging was performed in single track mode with a long pass 505 nm filter.

Cells were manually located on the coverslip with a FITC filter and mercury lamp excitation source. To determine the height of the cells, a z-stack was acquired using a 40x air objective with a numerical aperture of 0.75 and a pinhole size of 1 Airy unit. In order to minimize photobleaching, scanning was performed in bidirectional lines with no averaging at the fastest scan speed possible in order to reduce the time for

acquiring a full z-stack. The time to acquire a single image was set to less than 300 msec and a full z-stack was collected in less than a minute.

The z-stack information was used to select a focal plane approximately 2 μm from the coverslip surface for time-lapse imaging during exposure of the cells to hypertonic solution. Time series images were collected at a rate of 0.5 Hz while cells were being exposed to solutions at a flow rate of 200 mL/h. Cells were initially exposed to isotonic PBS for 1 min, switched to hypertonic for 1 min, and returned to isotonic PBS for a final 1 min. Fluid flow caused minor bowing in the coverslip which resulted in deviations in the focal plane from the initial set-up. To compensate for these deviations, during the initial 10–20 s of imaging with isotonic flow, the detector gain and amplifier offset were adjusted to minimize saturation and maintain the maximum fluorescence dynamic range. The pinhole diameter was varied between 57 μm and 513 μm (i.e., between 0.5 and 4.5 Airy units), and time series were collected for each pinhole diameter.

Data Analysis

Time series images were exported as tiff images using the LSM 510 (Carl Zeiss Inc, Thornwood, NY) software and converted to multipage tiff files using Phantom 663 imaging software (Vision Research Inc, Wayne, NJ). The average fluorescence intensity for each image was determined using ImagePro software (Media Cybernetics, Bethesda, MD). Data was corrected for non-volume-dependent fading of fluorescence (e.g., photobleaching, dye leakage) by fitting an exponential decay model to measurements made while cells were in equilibrium with isotonic solution, as described previously [19, 24]. The nondimensional cell fluorescence $\overline{F}$ was determined by normalizing the fluorescence intensity measurements to the best-fit exponential model.

Membrane water permeability was determined using methods similar to those published previously [24, 25]. Briefly, membrane water transport was described using the following model

$$\frac{d\overline{V}_w}{dt} = \overline{L}_p RT\left(\frac{\rho_w M_0}{\overline{V}_w} - \rho_w M_e\right) \quad (1)$$

where R is the ideal gas constant, T is the absolute temperature, $\overline{L}_p$ is the effective water permeability, M_0 is the isotonic osmolality, M_e is the osmolality of the extracellular solution, $\overline{V}_w$ is the nondimensional cell water volume, and ρ_w is the density of water (assumed to be 1 kg/L). A linear relationship was assumed between $\overline{V}_w$ and $\overline{F}$

$$\left(\overline{F} - 1\right) = a\left(\overline{V}_w - 1\right) \quad (2)$$

where a is a constant. Equations (1) and (2) were combined to obtain the following model:

$$\frac{d\overline{F}}{dt} = \overline{L}_p RT\left(\frac{a^2\rho_w M_0}{F + a - 1} - a\rho_w M_e\right) \quad (3)$$

To determine best-fit values for $\overline{L}_p$ and a, we used the experimental data directly after exposure to hypertonic solution. A step change in solution composition was assumed when the hypertonic solution first reached the cells. The time at which this step change occurred was calculated using the switch time recorded by the pumps, the length of tubing from the Y-connector to the channel inlet, and the flow rate. Equation 3 was numerically integrated and the sum of the squared residuals between the measured and predicted values of $\overline{F}$ was computed. This error was minimized by systematically iterating the values of $\overline{L}_p$ and a to determine best-fit values.

Results

Images collected from a z-stack reconstruction of a group of cells are shown in Fig. 1. These images were used to estimate the approximate height of the cells to be 5–6 μm. Eleven images were included in the z-stack, each with an optical slice thickness of 2.2 μm spaced 0.7 μm apart so that imaged sections of the cells overlap. The brightest image was the 6th image collected in the z-stack. This image was estimated to be 3–4 μm away from the coverslip. We chose to center our time-series images approximately 2 μm away from the coverslip, which ensured that cell images would be acquired when the cells were in the shrunken state.

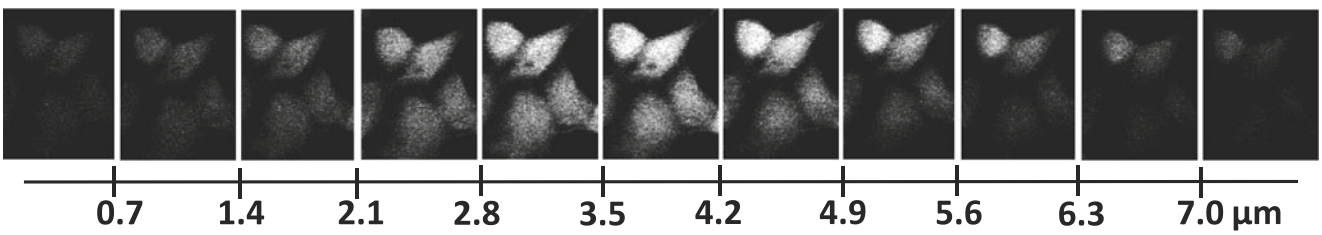

Fig. 1 Confocal images for z-stack reconstruction. Measurements represent the step distance within the z-stack

The cells shown in Fig. 1 were imaged during exposure to hypertonic solution and the resulting measurements of the nondimensional cell fluorescence $(\overline{F})$ are shown in Fig. 2 for various pinhole diameters. There was a clear difference in the magnitude of $\overline{F}$ when the cells were in hypertonic and isotonic solutions, with the exception of a pinhole diameter of 285 μm, which corresponds with an optical slice thickness of 5 μm. This demonstrates that in general, cell shrinkage upon exposure to hypertonic conditions was associated with a change in fluorescence. However, the magnitude of this change in fluorescence was dependent on the pinhole diameter. For small pinhole diameters, the fluorescence increased upon exposure to hypertonic conditions, with the largest increase in fluorescence occurring when the pinhole diameter was at a minimum of 57 μm (which corresponds with an optical slice thickness of 1.5 μm). In contrast, large pinhole diameters were associated with a decrease in fluorescence upon exposure to hypertonic conditions. A maximum decrease in fluorescence was observed with a pinhole diameter of 513 μm (which corresponds with an optical slice thickness of 9.1 μm).

Table 1 gives estimates for the parameters $\overline{L}_p$ and a obtained by fitting the data shown in Fig. 2 with the permeability model (Eq. 3). For a pinhole diameter of 285 μm, the change in cell fluorescence upon exposure to hypertonic conditions was so small that it was indistinguishable from the noise in the data, and consequently the best-fit water permeability in this case is probably not very accurate. For all of the other pinhole diameters, permeability estimates varied by less than 2-fold. At the highest and lowest pinhole diameters used in this study, permeability estimates only differed by 30 %, resulting in an average value of approximately $\overline{L}_p = 6 \times 10^{-8}$ $\mathrm{Pa^{-1}s^{-1}}$. This value is comparable to water permeability values reported for cultured endothelial cells in previous studies [19, 25].

The parameter a characterizes the relationship between cell volume and fluorescence, with negative values indicating an increase in fluorescence when the cell shrinks and positive values indicating a decrease in fluorescence when the cell shrinks (see Eq. 2). As shown in Table 1, negative a-values were observed when the pinhole diameter was smaller than 285 μm and positive a-values were observed for pinhole diameters larger than 285 μm. To quantitatively examine the relationship between cell fluorescence and cell volume, the a-values in Table 1 were used with Eq. 2 to calculate the equilibrium cell fluorescence under hypertonic conditions. The resulting values of the equilibrium cell fluorescence are plotted against the optical slice thickness in Fig. 3. Linear regression to the data yielded a slope that was significantly less than zero (p=0.006) and a correlation coefficient of R^2= 0.88, which indicates that the equilibrium cell fluorescence and the optical slice thickness are negatively correlated.

Table 1 Best-fit parameters from permeability model (Eq. 3)

Pinhole diameter		Optical slice thickness (μm)	$\overline{L}_p \times 10^8 (\mathrm{Pa^{-1}s^{-1}})$	a
(Airy)	(μm)			
0.5	57	1.5	6.89	−1.07
1	114	2.2	7.92	−0.74
1.5	171	3.2	10.2	−0.38
2.5	285	5	2.94	0.04
3.5	399	7.1	5.12	0.24
4.5	513	9.1	5.12	0.31

Discussion

It has been shown in previous studies that calcein fluorescence is quenched by molecules present in the cytosol [14]. This property of calcein would be expected to affect the fluorescence emitted when a cell shrinks or swells. For instance, when cells are exposed to a hypertonic solution they will shrink due to the loss of water required to reach

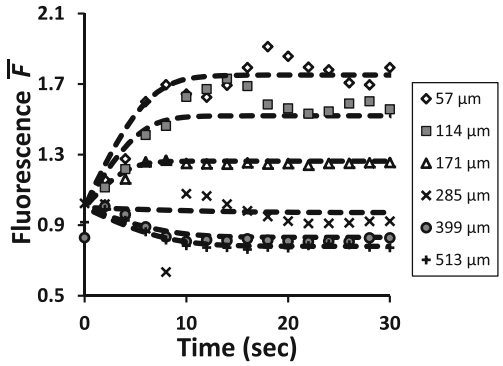

Fig. 2 Response of cell fluorescence after exposure to hypertonic conditions for various pinhole diameters. Best-fit trends (*dashed lines*) were determined using the permeability model (Eq. 3)

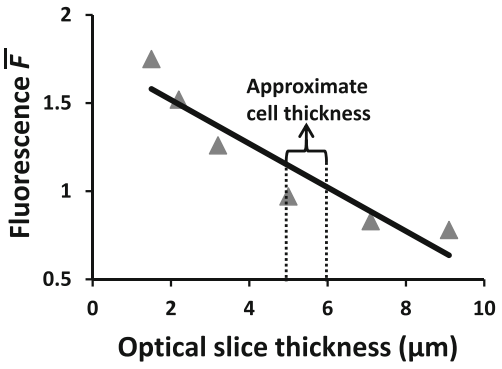

Fig. 3 Effect of optical slice thickness on the equilibrium fluorescence after exposure of a group of cells with a thickness of 5–6 μm to hypertonic conditions. The *line* shows a linear regression to the data. The approximate cell thickness is shown for reference (*dotted lines*)

osmotic equilibrium. As the cell volume decreases, calcein fluorophores trapped in the cytoplasm have more interactions with intracellular quenchers, resulting in a decrease in the amount of fluorescence that is emitted. Many studies have used wide-field epifluorescence imaging techniques with calcein as a volume indicator to study changes in cell volume [4–6, 9, 11–14, 16]. These studies have shown that as cell volume decreases, there is a corresponding decrease in fluorescence intensity. However, the exact opposite result has been observed in studies that have used confocal microscopy [7, 15, 17, 18].

The differences in the fluorescence response that have been observed using wide-field and confocal microscopy can be explained in terms of the differences between these two imaging modalities. When capturing wide-field images, fluorescence is collected from a relatively thick sample section. If the optical slice thickness is greater than the thickness of the cell, then fluorescence emission will reach the detector no matter where the fluorophores are located within the cell. Thus, the number of fluorophores being imaged is approximately the same before and after hypertonic exposure, and a decrease in fluorescence would be expected due to quenching. However, confocal images correspond with fluorescence from a relatively thin sample section. When the cell shrinks, fluorophores become concentrated in the cell and the quantity contained within the imaging section increases. This introduction of fluorophores into the focal plane would be expected to overwhelm the fluorescence quenching taking place, resulting in an overall increase in fluorescence with cell shrinkage.

Our data is consistent with this description of the fluorescence response. When the optical section was thick (≥7.1 μm) cell shrinkage caused the fluorescence to decrease, as expected for fluorescence quenching. On the other hand, when the optical section was thin (≤3.2 μm) cell shrinkage caused the fluorescence to increase, which is consistent with an increase in the number of calcein molecules within the imaged volume. The approximate thickness of the cells that we investigated in this study was 5–6 μm under isotonic conditions. The relationship between the fluorescence response and the cell thickness is illustrated in Fig. 3. This figure shows that when the optical section thickness was at least 20 % greater than the cell height, a decrease in fluorescence was observed, and when optical section thickness was about half the cell height (or thinner), an increase in fluorescence was observed.

The results of this study have implications for the development of methods to measure the permeability properties of cells within three-dimensional tissue. In particular, it may be possible to estimate permeability properties by using confocal microscopy to quantify the calcein fluorescence at a specific depth within a tissue sample after exposure to a hyper- or hypotonic solution. The results of the present study show that it will be important to consider the pinhole diameter – and the concomitant optical section thickness – when conducting this type of experiment.

Conclusion

Previous studies provide conflicting results indicating that calcein fluorescence can both increase and decrease when cell shrinkage is induced, depending on whether confocal or wide-field microscopy is used. In this study, we have demonstrated that this discrepancy is a result of the optical slice thickness and its relationship to the height of the cells being imaged. Our results provide guidelines for selection of optical slice thickness for measuring volume changes in calcein-stained cells, potentially facilitating the development of methods for measuring cell membrane permeability in three-dimensional tissues.

References

1. McGrath JJ (1997) Quantitative measurement of cell membrane transport: technology and applications. Cryobiology 34:315–334
2. Verkman AS (2000) Water permeability measurement in living cells and complex tissues. J Membr Biol 173:73–87
3. Verkman AS, VanHoek AN, Ma TH, Frigeri A, Skach WR, Mitra A, Tamarappoo BK, Farinas J, Van Hoek AN (1996) Water transport across mammalian cell membranes. Am J Physiol, Cell Physiol 270:C12–C30
4. Ruiz-Ederra J, Verkman AS (2006) Accelerated cataract formation and reduced lens epithelial water permeability in aquaporin-1-deficient mice. Invest Ophthalmol Vis Sci 47:3960–3967
5. Mitchell CH, Fleischhauer JC, Stamer WD, Peterson-Yantorno K, Civan MM (2002) Human trabecular meshwork cell volume regulation. Am J Physiol, Cell Physiol 283:315–326
6. Yellowley CE, Hancox JC, Donahue HJ (2002) Effects of cell swelling on intracellular calcium and membrane currents in bovine articular chondrocytes. J Cell Biochem 86:290–301
7. Zelenina M, Zelenin S, Bondar AA, Brismar H, Alexander A, Aperia A (2002) Water permeability of aquaporin-4 is decreased by protein kinase C and dopamine. Am J Physiol Renal Physiol 283:F309–F318
8. Altamirano J, Brodwick MS, Alvarez-Leefmans FJ (1998) Regulatory volume decrease and intracellular Ca2+ in murine neuroblastoma cells studied with fluorescent probes. J Gen Physiol 112:145–160
9. Capo-Aponte JE, Iserovich P, Reinach PS, Capó-Aponte JE (2005) Characterization of regulatory volume behavior by fluorescence quenching in human corneal epithelial cells. J Membr Biol 207:11–22
10. Crowe WE, Altamirano J, Huerto L, Alvarez-Leefmans FJ (1995) Volume changes in single N1E-115 neuroblastoma cells measured with a fluorescent probe. Neuroscience 69:283–296
11. Levin MH, Verkman AS (2004) Aquaporin-dependent water permeation at the mouse ocular surface: in vivo microfluorimetric measurements in cornea and conjunctiva. Invest Ophthalmol Vis Sci 45:4423–4432
12. Hamann S, Herrera-Perez JJ, Bundgaard M, Alvarez-Leefmans FJ, Zeuthen T (2005) Water permeability of Na+—K+—2Cl- cotransporters in mammalian epithelial cells. J Physiol (Lond) 568:123–135

13. Hamann S, Kiilgaard JF, Litman T, Alvarez-leefmans FJ, Winther BR, Zeuthen T (2002) Measurement of cell volume changes by fluorescence self-quenching. J Fluoresc 12:139–145
14. Solenov E, Watanabe H, Manley GT, Verkman AS (2004) Sevenfold-reduced osmotic water permeability in primary astrocyte cultures from AQP-4-deficient mice, measured by a fluorescence quenching method. Am J Physiol, Cell Physiol 286:426–432
15. Sonnentag T, Siegel WK, Bachmann O, Rossmann H, Mack A, Wagner HJ, Gregor M, Seidler U (2000) Agonist-induced cytoplasmic volume changes in cultured rabbit parietal cells. Am J Physiol Gastrointest Liver Physiol 279:G40–G48
16. Li L, Zhang H, Ma T, Verkman AS (2009) Very high aquaporin-1 facilitated water permeability in mouse gallbladder. Am J Physiol Gastrointest Liver Physiol 296:816–822
17. Zelenina M, Brismar H (2000) Osmotic water permeability measurements using confocal laser scanning microscopy. Eur Biophys J 29:165–171
18. Fenton RA, Moeller HB, Zelenina M, Snaebjornsson MT, Holen T, MacAulay N (2010) Differential water permeability and regulation of three aquaporin 4 isoforms. Cell Mol Life Sci 67:829–840
19. Fry AK, Higgins AZ (2012) Measurement of cryoprotectant permeability in adherent endothelial cells and applications to cryopreservation. Cell Mol Bioeng 5:287–298
20. Gao DY, Liu J, Liu C, McGann LE, Watson PF, Kleinhans FW, Mazur P, Critser ES, Critser JK (1995) Prevention of osmotic injury to human spermatozoa during addition and removal of glycerol. Hum Reprod 10:1109–1122
21. Benson JD, Kearsley AJ, Higgins AZ (2012) Mathematical optimization of procedures for cryoprotectant equilibration using a toxicity cost function. Cryobiology 64:144–151
22. Karlsson JOM, Younis AI, Chan AWS, Gould KG, Eroglu A (2009) Permeability of the rhesus monkey oocyte membrane to water and common cryoprotectants. Mol Reprod Dev 76:321–333
23. Mukherjee IN, Song YC, Sambanis A (2007) Cryoprotectant delivery and removal from murine insulinomas at vitrification-relevant concentrations. Cryobiology 55:10–18
24. Higgins AZ, Karlsson JOM (2010) Analysis of solution exchange in flow chambers with applications to cell membrane permeability measurement. Cell Mol Bioeng 3:269–285
25. Higgins AZ, Karlsson JOM (2012) Comparison of cell membrane water permeability in monolayers and suspensions. Cryo-Letters 33:95–106